RSC Advances

PAPER

View Article Online
View Journal | View Issue

Cite this: *RSC Adv.*, 2014, **4**, 40638

Nonenzymatic hydrogen peroxide biosensor based on four different morphologies of cuprous oxide nanocrystals

Yanmei Zhong,[a] Yancai Li,*[ab] Shunxing Li,[ab] Shuqing Feng[a] and Yayun Zhang[a]

In this work, we synthesized four different morphologies of cuprous oxide (Cu_2O) nanocrystals (cube, rhombic dodecahedra, octahedra, and extended hexapod) by a hydrothermal method. Then, the four different morphologies of Cu_2O were immobilized separately on a glassy carbon electrode (GCE) to construct a non-enzymatic hydrogen peroxide (H_2O_2) biosensor. We systematically explored the electrocatalytic activities of the four different Cu_2O nanocrystals towards H_2O_2, which are strongly dependent on the shape of the Cu_2O nanocrystals. It is shown that the modified electrodes exhibited excellent electrocatalysis for H_2O_2 reduction by electrochemical experiments. Moreover, the {111}-bounded extended hexapod Cu_2O, {111}-bounded octahedral Cu_2O and the {110}-bounded rhombic dodecahedral Cu_2O nanocrystals are significantly more active than the {100}-bounded cubic Cu_2O nanocrystals, as the {111} and {110} face contain copper atoms on the surface with dangling bonds, and are expected to interact more strongly with negatively charged ions or molecules.

Received 19th May 2014
Accepted 19th August 2014

DOI: 10.1039/c4ra04718d

www.rsc.org/advances

1. Introduction

Research on the quantitative detection of H_2O_2 has been given considerable attention, since H_2O_2 is widely used as an oxidizing agent in the fields of chemistry, biology, pharmaceutical analysis, and environmental protection.[1,2] The electrochemistry method is a promising method because of its high sensitivity and selectivity, rapid response, and low cost, simple instrumentation, and good quantitative ability.[3–5] However, regardless of the electrocatalytic oxidation or electrocatalytic reduction needs a kind of stable and high performance electrocatalyst, which including metal nanoparticles,[6] metal hexacyanoferrate,[7,8] metal oxide.[9–11] Therefore, metal oxide with reusable, inexpensive, good stability which can be directly detected substance without enzyme materials has been widely used in design new non-enzymatic sensor.

Thus, researchers have been focusing on the synthesis of metal oxide as electrocatalyst to electrocatalytic reduction of H_2O_2 in recent years.[12–14] In addition, many studies have revealed that the electrocatalytic ability of metal nanocrystals which strongly depend on their size, shape, composition and structure.[15–17] Such as the influence of the morphology of Au nanocrystals on its electrocatalytic oxidation toward glucose was studied by Tang *et al.*,[18] Herrero *et al.* evaluated the catalytic properties of different shape-controlled platinum nanoparticles for oxygen reduction reaction,[19] and Schoonmaker *et al.* reported the Fe {111} face was found to be the most active, the activity ratio being 418 : 25 : 1 for the Fe {111}, Fe {100} and Fe {110} planes,[20] *etc.* However, little researches of the influence on metal oxide morphology towards the electrocatalytic ability. Therefore, studying the influence of the morphology of metal oxide on its electrochemical properties is very important. Furthermore, the morphology effect mainly originates from the different crystal planes exposed on the nanocrystals surface. Generally speaking, nanocrystals with high-index facets are found to possess dramatic high catalytic activity.[21,22] However, nanocrystals with high-index facets commonly have a high surface energy, which lead to possible structural instability and decrease repeated utilization of their catalytic activity.[23] While the nanocrystals with low-index facets have both high activity and good stability.[24,25] In addition, the Cu_2O nanocrystals were already used to modify electrode for detecting H_2O_2 and the results showed that a high electrochemical performance.[26,27] Furthermore, studying the effect of morphology and specific surface area of the Cu_2O on electrochemical properties is also necessary. Consequently, three types of low-index planes of Cu_2O, including {111}, {110} and {100} planes are selected as the research objects in our work.

In this study, the cubic Cu_2O which have six {100} faces, the extended hexapod and the octahedral Cu_2O particles, which have twenty four and eight {111} faces, the rhombic dodecahedral Cu_2O, which have {100}, {110} and {111} faces,[28,29] were synthesized and investigated the influence of three kinds of crystal facets on electrocatalytic properties toward H_2O_2.

---

[a] College of Chemistry and Environment, Minnan Normal University, Zhangzhou 363000, China. E-mail: liyancai@mnnu.edu.cn

[b] Fujian Province Key Laboratory of Modern Analytical Science and Separation Technology, Minnan Normal University, Zhangzhou 363000, China

2. Experimental

2.1 Reagents and materials

Copper(II) chloride dehydrate ($CuCl_2 \cdot 2H_2O$, 99.0%), sodium dodecyl sulfate (SDS, 98.5%) and hydroxylamine hydrochloride ($NH_2OH \cdot HCl$, 99.99%) were purchased from Aladdin industrial. H_2O_2 solution (30%) was purchased from Chongqing Chuandong chemical company. All other chemicals were of analytical grade and were used without further purification. All solutions were made up with double-distilled water.

2.2 Apparatus

Scanning electron microscopy (SEM) was provided with Hitachi S-4800; Powder XRD patterns were recorded on a Pan-altical X'Pert-pro MPD X-ray power diffractometer, using Cu Kα radiation; the mode of specific surface and porosity analyzer is ASAP2020 instrument. The electrochemical experiments were carried out with a CHI 650C electrochemical workstation (Shanghai Chenhua Instruments) with a conventional three-electrode cell, the modified or unmodified glassy carbon electrode (GCE, 3 mm diameter) was used as the working electrode, and the Pt wire and Ag/AgCl (3.0 M KCl) electrode were used as the counter and reference electrodes, respectively.

2.3 Synthesis of the Cu_2O nanocrystals

The four different morphologies of Cu_2O nanocrystals were synthesized by a hydrothermal method according to previously reported with minor modification.[29,30] In brief, four beakers (150 mL) were prepared which labeled a, b, c, d, and were added to 95.8, 91, 91, 80.2 mL of deionized water, respectively. And then, 1, 1, 1, 5 mL of 0.1 M $CuCl_2$ and 2, 2, 0.5, 1.8 mL of 1.0 M NaOH solution were added to the four beakers (a, b, c, d) in order with vigorous stirring. The solution turned light blue immediately, indicating that there is generated $Cu(OH)_2$ precipitate. Next, 0.88 g of SDS powder was added with vigorous stirring of the four beakers until the powder dissolved. Finally, 1.2, 6, 13 mL of 0.2 M $NH_2OH \cdot HCl$ was mixed with the solutions in the beakers of a, b, d; and 7.5 mL of 0.2 M $NH_2OH \cdot HCl$ was titrated into the beaker c. Finally, the samples were centrifuged at 5000 rpm for 3 min (Rotina 420R centrifuge) and obtained precipitates. The brick-red precipitates were centrifuged twice more in ethanol and deionized water and then were dispersed in 1 mL of ethanol for the following experiments.

2.4 Preparation of the Cu_2O nanocrystals modified electrode

GCE was polished before each experiment with 1, 0.3 and 0.05 μm alumina powder, respectively, rinsed thoroughly with ethanol and double distilled water. 7.2 mg extended hexapod Cu_2O nanocrystals were dissolved in a mixture of 0.1 mL Nafion and 0.9 mL double-distilled water. Under ultrasonic mixing for a few minutes, a brick-red suspension was obtained. Then, 10 μL extended hexapod Cu_2O mixture was coated on a cleaned GCE and allowed to dry in air to fabricate the extended hexapod Cu_2O/Nafion/GCE. A similar procedure was employed to fabricate the other Cu_2O modified electrodes.

3. Results and discussion

3.1 Characterization of the Cu_2O nanocrystals

The shapes and particle size of the four types Cu_2O nanocrystals can be clearly observed by SEM. As shown in Fig. 1. Fig. 1A–D severally indicated the morphology of the nanocube, the octahedra, the rhombic dodecahedra and the extended hexapod Cu_2O nanocrystals. The insets of SEM are enlarged view of a single Cu_2O nanocrystal of the four morphologies. As shown in these images, the single crystalline nature and sharp faces of these nanocrystals are evidently observed. Moreover, the average particle size was all approximate to 500 nm and evidently the extended hexapod Cu_2O nanocrystals > the octahedra > the rhombic dodecahedra > the nanocube in order.

Fig. 2 displays the XRD patterns of the four different Cu_2O nanocrystals, the diffraction patterns clearly show the difference of relative intensities of the (111), (110) and the (200) peaks. As expected, nanocube present an extraordinary strong (200) reflection peak and a weak (111) reflection peak; the rhombic dodecahedraalso presents a weak (111) reflection peak; the octahedral and extended hexapod Cu_2O particles exhibit an enhanced (111) reflection peak in turn. The progressively increasing of the (111) reflection peak intensity demonstrated that more {111} surfaces of the nanocrystals are formed. That is to say, the extended hexapod Cu_2O particles possess most {111} surfaces. The rhombic dodecahedral Cu_2O also show a weak (110) reflection peak, which indicate that the rhombic dodecahedral Cu_2O have {110} surfaces. Therefore, the four different

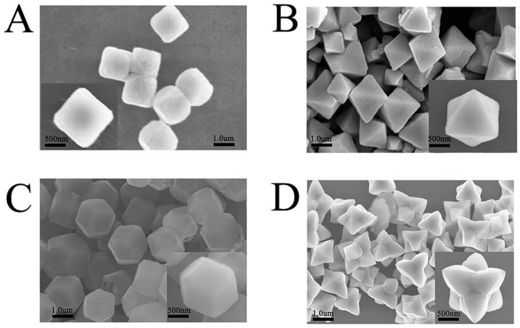

Fig. 1 SEM images of the nanocubic Cu_2O (A), the octahedral Cu_2O (B), the rhombic dodecahedral Cu_2O (C) and the extended hexapod Cu_2O (D) nanocrystals.

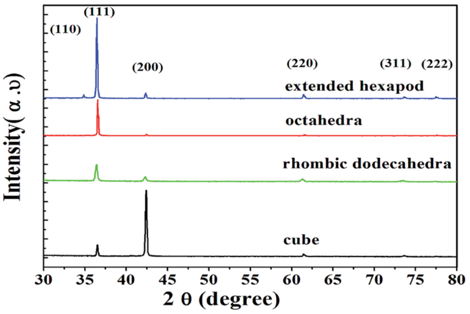

Fig. 2 XRD patterns of the four different Cu_2O nanocrystals.

Cu_2O may possess nice electrochemical performance and the influence of the three kinds of crystal faces on the electrocatalytic reduction toward H_2O_2 was studied in the following experiments.

3.2 Electrochemical characterization

Electrochemical impedance spectroscopy (EIS) can analyze the properties of the electrode surface during the modification process, so we carried out EIS of the four electrodes with a frequency ranging from 0.01 to 100 kHz in 0.1 M KCl electrolyte solution containing 5 mM $Fe(CN)_6{}^{4-/3-}$, as shown in Fig. 3. The proposed equivalent circuits of the EIS data was displayed in the inset of Fig. 3, which correspond to the modified electrodes. R_s, R_c and R_{ct} are the solution, coating and charge transfer resistances, respectively. A constant phase element (CPE) is attributed to a charge transfer process replacing the double layer capacity (C_{dl}). In equivalent circuits, CPEe and CPEc are the constant phase elements of the electrode and coating, respectively. In this circuit, the impedance of a Faradaic reaction consists of an active charge transfer resistance R_{ct} and a specific electrochemical element of diffusion R_w (Warburg element). From the EIS curve, we can conclude that the four kinds of Cu_2O nanocrystals have been attached to the electrode surface and the electron transfer resistance of the extended hexapod Cu_2O is much less than the other three kinds of Cu_2O. Therefore, the extended hexapod Cu_2O/Nafion/GCE should have higher electrochemical activity than the others Cu_2O/Nafion/GCE.

3.3 Electrochemical performance towards H_2O_2

Fig. 4 shows the cyclic voltammograms (CVs) of the four different morphology of Cu_2O/Nafion/GCE in the absence and presence of 0.6 mM H_2O_2 in N_2-saturated 0.1 M pH 7.4 PBS at scan rate of 150 mV s^{-1}. There is a strong redox peaks between −0.3 and −0.02 V in the four modified electrodes (curve a of Fig. 4A–D), the anodic and cathodic peak can be ascribed to the oxidation of Cu_2O to CuO and the reduction of CuO to Cu_2O.[31]

The reaction equation can be expressed as:

$$2CuO + H_2O + 2e \rightarrow Cu_2O + 2OH^- \quad (1)$$

$$Cu_2O + H_2O_2 \rightarrow 2CuO + H_2O \quad (2)$$

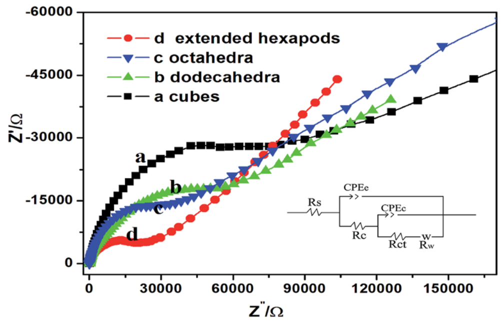

Fig. 3 EIS of the nanocubic Cu_2O/Nafion/GCE (a), the rhombic dodecahedral Cu_2O/Nafion/GCE (b), the octahedral Cu_2O/Nafion/GCE (c) and the extended hexapod Cu_2O/Nafion/GCE (d) in 0.1 M KCl electrolyte solution containing 1 mM $Fe(CN)_6{}^{4-/3-}$, the applied ac frequency range: 0.1 Hz to 100 kHz. Inset is the equivalent circuits of the EIS.

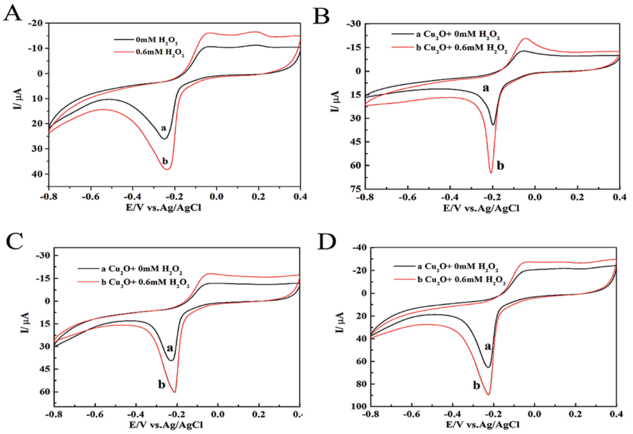

Fig. 4 CVs of the nanocubic Cu_2O/Nafion/GCE (A), the rhombic dodecahedral Cu_2O/Nafion/GCE (B), the octahedral Cu_2O/Nafion/GCE (C) and the extended hexapod Cu_2O/Nafion/GCE (D) in 5 mL 0.1 M pH 7.4 PBS in absence (a) and presence (b) of H_2O_2, scan rate: 150 mV s^{-1}.

The reduction peak currents of the four different Cu_2O nanocrystals modified electrodes increased obviously when H_2O_2 was added (curve b of Fig. 4A–D) and the cathodic peak current increased the multiple of 12.3, 21.0, 24.4, 29.8, respectively. The experimental results demonstrated that the as-synthesized four kinds of Cu_2O have electrocatalytic activity for the H_2O_2 reduction. Moreover, the order of reduction peak currents increase of these four electrodes toward H_2O_2 is the extended hexapod Cu_2O > the octahedral Cu_2O > the rhombic dodecahedral Cu_2O > the cubic Cu_2O. That means, the electrocatalytic ability toward H_2O_2 is the extended hexapod Cu_2O > the octahedral Cu_2O > the rhombic dodecahedral Cu_2O > the cubic Cu_2O. This can be attributed to the presence of dangling bonds from the copper atoms surface, which possess positively charged from the Cu_2O crystals bounded by the {111} and {110} faces; whereas those {100} facets which the cubic Cu_2O containing are electrical neutral, and can not interact well with OH^- in the solution and present inertness. In addition, the amount of {111} facets of different Cu_2O crystals are the extended hexapod Cu_2O > the octahedral Cu_2O > the rhombic dodecahedra Cu_2O orderly, besides, the cubic Cu_2O nanocrystals have no {111} facets. Therefore, the extended hexapod Cu_2O revealed best electrocatalytic ability toward H_2O_2.

Fig. 5A displays the CVs of the extended hexapod Cu_2O/Nafion/GCE at different scan rates in 0.1 M pH 7.4 PBS without H_2O_2. The redox peak current increases with increasing scan rate from 100 mVs^{-1} to 500 mV s^{-1}. Fig. 5B shows the linearly relationship between the redox peak currents and square root of the scan rate (I_{pa} (μA) = 9.86 − 102.10$v^{1/2}$ (V s^{-1}), R = 0.999; I_{pc} (μA) = −16.89 + 218.34$v^{1/2}$ (V s^{-1}), R = 0.999), indicating that the redox process follows a diffusion-controlled mechanism.

Fig. 6A shows *I*–*t* curves of the four different morphologies of Cu_2O modified electrodes in 0.1 M pH 7.4 PBS for the addition of 0.05 mM H_2O_2. It is clear that four electrodes have rapid amperometric response to H_2O_2, and the current response of the extended hexapod Cu_2O > the octahedral Cu_2O > the rhombic dodecahedral Cu_2O > the cubic Cu_2O. This also

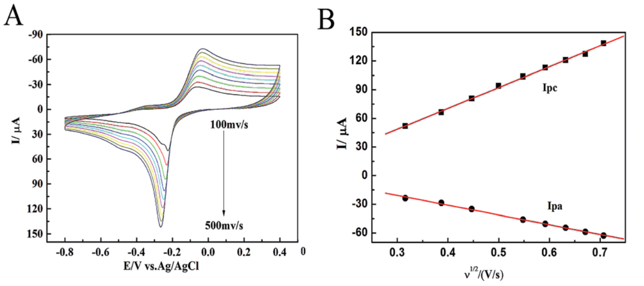

Fig. 5 (A) CVs of the extended hexapod Cu_2O/Nafion/GCE at different scan rates: 100, 150, 200, 250, 300, 350, 400, 450, 500 mV s^{-1} in 0.1 M pH 7.4 PBS without H_2O_2, (B) the relationship between the redox peak currents and square root of the scan rates.

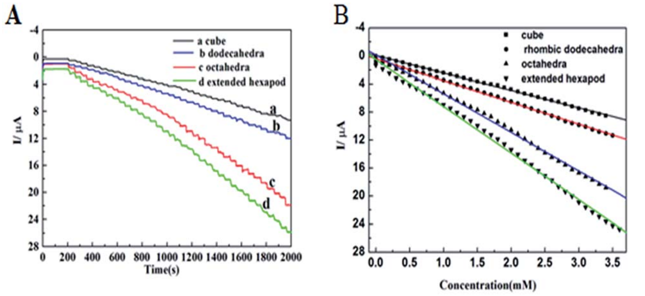

Fig. 6 (A) Amperometric response of the four different Cu_2O modified electrodes upon successive additions of H_2O_2 to 5 mL 0.1 M pH 7.4 PBS at an applied potential of −0.2 V, (B) the corresponding calibration curves of oxidation currents *vs.* H_2O_2 concentrations.

demonstrates that there is a rapid and sensitive response to H_2O_2 reduction of the extended hexapod Cu_2O/Nafion/GCE. The four calibration curves as shown in Fig. 6B, the H_2O_2 concentration showed a terrific linear relationship with the response current on the four electrodes. The linear range, the limits of detection and sensitivities of the four kinds of Cu_2O/Nafion/GCE are summed up in Table 1. From the Table 1, the linear range and sensitivities of the four kinds of Cu_2O increase and the limits of detection reduce in order.

The best electrocatalytic activity of the extended hexapod Cu_2O can be attributed to the {111} faces, which have higher surface energy and a greater density of the "Cu" dangling bonds and expected to be more electrocatalytic active than the {100} faces besides, {111}-bounded Cu_2O have more edges and corners, which could improve electrocatalytic activity. Furthermore, Cu_2O crystals bounded by the {111} faces contain positively charged copper atoms at the surfaces, whereas those bounded by the {100} faces such as the cube are electrically neutral.[30] These factors can effectively increase the electrocatalytic active areas and promote electron transfer in the reduction of H_2O_2. These all suggest that Cu_2O nanocrystals with more {111} facets can serve as more efficient electrocatalyst. That is to say, {111}-bounded the extended hexapod Cu_2O with the highest surface energy and the greatest density of the "Cu" dangling bonds and contain positively charged copper atoms at the surfaces could be chosen to construct the non-enzyme sensor to detect H_2O_2 in the future.

3.6 The effect of the specific surface area of the four kinds of Cu_2O

The specific surface area of the four kinds of Cu_2O nanocrystals was also investigated, as shown in Table 2. Firstly, the result demonstrated that the four kinds of Cu_2O all possess large specific surface area, which can explain its good electrocatalytic effect to H_2O_2 reduction. In addition, as can be expected, the order of the specific surface area is the extended hexapod Cu_2O < the octahedral Cu_2O < the rhombic dodecahedral Cu_2O < the cubic Cu_2O. In other words, the largest extended hexapod Cu_2O have the smallest specific surface area; however, it possesses the best electrocatalytic activity to H_2O_2 reduction as shown in the above electrochemical results. This can also prove that the well electro-catalytic effect of the extended hexapod Cu_2O mainly depends on its {111} faces rather than the specific surface area, which is consistent with our former conclusions.

3.7 Stability of the four kinds of Cu_2O/Nafion/GCE

It is well known that the stability was also a important parameter for electrochemical sensors. The CVs of the four kinds of Cu_2O/Nafion/GCE were performed for H_2O_2 reduction every 48 h and the modified electrodes drying in air, as show in Fig. 7 The results clearly indicate that the low-index planes of (111)-extended hexapod Cu_2O/Nafion/GCE is the most stable for H_2O_2 reduction, which suggests that (111)-extended hexapod Cu_2O/Nafion/GCE possesses the best stability.

Table 2 The specific surface area of the four kinds of Cu_2O

Four kinds of Cu_2O	BET surface area (m^2 g^{-1})
Cubic Cu_2O	29.3
Rhombic dodecahedral Cu_2O	18.8
Octahedral Cu_2O	15.9
Extended hexapod Cu_2O	15.3

Table 1 Analytical performances of the four kinds of Cu_2O based non-enzymatic H_2O_2 biosensors

Four kinds of Cu_2O	Sensitivity (μA μM^{-1} cm^{-2})	Linear range (mM)	Detection limit (μM)
The cubic Cu_2O	0.0352	0.05–3.4	12.4
The rhombic dodecahedral Cu_2O	0.0440	0.05–3.4	12.3
The octahedral Cu_2O	0.0783	0.05–3.5	6.1
The extended hexapod Cu_2O	0.0944	0.05–3.6	5.4

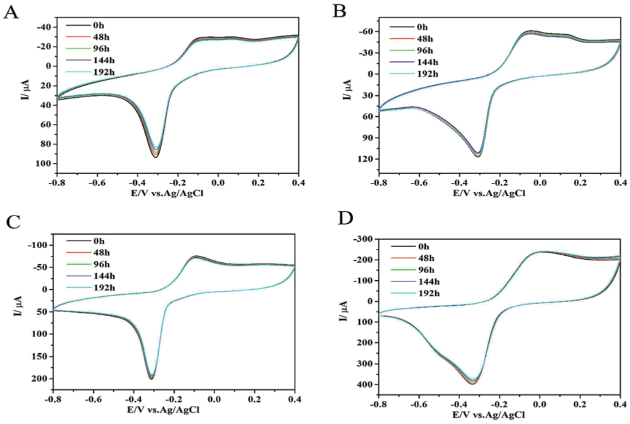

Fig. 7 The CVs of the four kinds of modified electrodes for 0.4 mM H_2O_2 in 5 mL 0.1 M pH 7.4 PBS every 48 h, the cubic Cu_2O/Nafion/GCE (A), the rhombic dodecahedral Cu_2O/Nafion/GCE (B), the octahedral Cu_2O/Nafion/GCE (C) and the extended hexapod Cu_2O/Nafion/GCE (D), scan rate: 150 mV s^{-1}.

4. Conclusions

Cu_2O nanocrystals of diversified shapes (cube, octahedra, rhombic dodecahedra, and extended hexapod) were synthesized and characterized by SEM and XRD. Their electrocatalytic properties for the detection of H_2O_2 which depend on the morphology were studied. As a result, {111}-bounded the extended hexapod, {111}-bounded octahedra and the rhombic dodecahedra Cu_2O nanocrystals, exposing the {110} facets, which contain surface copper atoms with dangling bonds, exhibit a good electrocatalytic reduction toward H_2O_2 in the solutions contain negative charge compared to the cubic Cu_2O with {100} facets which is electrical neutral. On the contrary, solutions containing positively charged molecules or ion can repel the crystals with {111} and {110} surfaces and make a significant amount of the crystals float to the top surface of the solution and will make that the reaction can not be performed.

Acknowledgements

This work was supported by the National Natural Science Foundation of China (21175115), the Program for New Century Excellent Talents in University, Natural Science Foundation of Fujian province in China (2012Y0065 and 2012J05031), and the Innovation Base Foundation for Graduate Students Education of Fujian Province.

Notes and references

1 R. C. Matos, J. J. Pedrotti and L. Angnes, *Anal. Chim. Acta*, 2001, **441**, 73–79.
2 D. J. Barrington and A. Ghadouani, *Environ. Sci. Technol.*, 2008, **42**, 8916–8921.
3 K. Zhang, L. Zhang, J. Xu, C. Wang, T. Geng, H. Wang and J. Zhu, *Microchim. Acta*, 2010, **171**, 139–144.
4 Z. Yin, J. Wu and Z. Yang, *Biosens. Bioelectron.*, 2011, **26**, 1970–1974.
5 K. Cui, Y. Song, Y. Yao, Z. Huang and L. Wang, *Electrochem. Commun.*, 2008, **10**, 663–667.
6 S. Guo, D. Wen, S. Dong and E. Wang, *Talanta*, 2009, **77**, 1510–1517.
7 N. A. Sitnikova, A. V. Borisova, M. A. Komkova and A. A. Karyakin, *Anal. Chem.*, 2011, **83**, 2359–2363.
8 Z. Wang, S. Sun, X. Hao, X. Ma, G. Guan, Z. Zhang and S. Liu, *Sens. Actuators, B*, 2012, **171**, 1073–1080.
9 A. Noorbakhsh and A. Salimi, *Electrochim. Acta*, 2009, **54**, 6312–6321.
10 W. D. Zhang, J. Chen, L. C. Jiang, Y. X. Yu and J. Q. Zhang, *Microchim. Acta*, 2010, **168**, 259–265.
11 A. Gu, G. Wang, X. Zhang and B. Fang, *Bull. Mater. Sci.*, 2010, **33**, 17–20.
12 B. Šljukic, C. E. Banks and R. G. Compton, *Nano Lett.*, 2006, **6**, 1556–1558.
13 S. G. Leonardi, D. Aloisio, N. Donato, P. A. Russo, M. C. Ferro, N. Pinna and G. Neri, *ChemElectroChem*, 2014, **1**, 617–624.
14 H. Lu, S. Yu, Y. Fan, C. Yang and D. Xu, *Colloids Surf., B*, 2013, **101**, 106–110.
15 J. Zeng, Q. Zhang, J. Chen and Y. Xia, *Nano Lett.*, 2009, **10**, 30–35.
16 V. Komanicky, H. Iddir, K. C. Chang, A. Menzel, G. Karapetrov, D. Hennessy, P. Zapol and H. You, *J. Am. Chem. Soc.*, 2009, **131**, 5732–5733.
17 J. Zhang, H. Yang, J. Fang and S. Zou, *Nano Lett.*, 2010, **10**, 638–644.
18 J. Wang, J. Gong, Y. Xiong, J. Yang, Y. Gao, Y. Liu, X. Lu and Z. Tang, *Chem. Commun.*, 2011, **47**, 6894–6896.
19 C. M. Sánchez-Sánchez, J. Solla-Gullón, F. J. Vidal-Iglesias, A. Aldaz, V. Montiel and E. Herrero, *J. Am. Chem. Soc.*, 2010, **132**, 5622–5624.
20 N. D. Spencer, R. C. Schoonmaker and G. A. Somorjai, *Nature*, 1981, **294**, 643–644.
21 N. Tian, Z.-Y. Zhou and S.-G. Sun, *J. Phys. Chem. C*, 2008, **112**, 19801–19817.
22 N. Tian, Z.-Y. Zhou, N.-F. Yu, L.-Y. Wang and S.-G. Sun, *J. Am. Chem. Soc.*, 2010, **132**, 7580–7581.
23 A. R. Tao, S. Habas and P. Yang, *Small*, 2008, **4**, 310–325.
24 Y. X. Chen, S. P. Chen, Z. Y. Zhou, N. Tian, Y. X. Jiang, S. G. Sun, Y. Ding and Z. L. Wang, *J. Am. Chem. Soc.*, 2009, **131**, 10860–10862.
25 X. Huang, S. Tang, H. Zhang, Z. Zhou and N. Zheng, *J. Am. Chem. Soc.*, 2009, **131**, 13916–13917.
26 S. Li, Y. Zheng, G. W. Qin, Y. Ren, W. Pei and L. Zuo, *Talanta*, 2011, **85**, 1260–1264.
27 Z. Gao, J. Liu, J. Chang, D. Wu, J. He, K. Wang, F. Xu and K. Jiang, *CrystEngComm*, 2012, **14**, 6639–6646.
28 Y. H. Won and L. A. Stanciu, *Sensors*, 2012, **12**, 13019–13033.
29 W. C. Huang, L. M. Lyu, Y. C. Yang and M. H. Huang, *J. Am. Chem. Soc.*, 2012, **134**, 1261–1267.
30 J. Y. Ho and M. H. Huang, *J. Phys. Chem. C*, 2009, **113**, 14159–14164.
31 Z. Yan, J. Zhao, L. Qin, F. Mu, P. Wang and X. Feng, *Microchim. Acta*, 2013, **180**, 145–150.